International Journal of Heat and Technology
Vol. 43, No. 6, December, 2025, pp. 2029-2037
Journal homepage: http://iieta.org/journals/ijht

Mixing Intensification Through Collision and Coalescence of Two Leidenfrost Drops

Hayato Masuda*, Koki Wada, Koki Takahashi, Hiroyuki Iyota

Department of Mechanical Engineering, Graduate School of Engineering, Osaka Metropolitan University, Osaka 5998531, Japan

Corresponding Author Email: Hayato-masuda@omu.ac.jp

https://doi.org/10.18280/ijht.430604

Received: 28 September 2025
Revised: 11 November 2025
Accepted: 19 November 2025
Available online: 31 December 2025

Keywords:
Leidenfrost drop, process intensification, drop collision, drop mixing, polymeric drop, drop reactor

ABSTRACT

The Leidenfrost drop is potentially suitable for process intensification due to the well-mixed and high-temperature field within the drop. To comprehensively evaluate the performance, we investigated the collision, coalescence, and mixing processes of two Leidenfrost drops. In particular, to clarify the effect of viscosity contrast, an ethanol (Et) drop colorized by methylene blue was ejected toward a stationary drop of either distilled water (DW), representing a low-viscosity system, or 0.1 wt% xanthan gum solution (XG), representing a high-viscosity system. Under various conditions of Weber number (*We*), the distilled water and ethanol drops coalesced immediately after collision; on the other hand, the xanthan gum and ethanol drops showed a delayed coalescence without a simultaneous coalescence after collision in low *We* conditions. After coalescence, the time required for mixing was measured by the change in the blue value within the drop. As a result, it was found that the mixing time depends not on *We* but on the drop viscosity. Nonetheless, the significantly rapid mixing was performed compared with stirred vessel systems, suppressing the increase in the energy consumption for the high viscosity liquid mixing due to the contactless interaction with any wall by levitation.

1. INTRODUCTION

Utilizing drops as a chemical reactor (i.e., drop reactor) has been gaining attention as a process intensification technology for material synthesis due to several advantages: (i) Short characteristic time for mixing, (ii) small size, and (iii) large specific area. Owing to these advantages, rapid manufacturing with high uniformity is realized. For example, the drop reactor has been applied to synthesize quantum dots [1], aerogels [2], and nanocrystals [3]. In these processes, drops of reactants collide with each other at the initial stage, coalesce, mix, and subsequently, the chemical reaction starts. Therefore, improving mixing after coalescence is crucial for realizing an inherent chemical reaction rate.

Focke et al. [4] showed both numerically and experimentally that the mixing process following the collision/coalescence of two drops in the air is insufficient under the moderate Weber number, *We*, condition; *We* is the ratio of inertial forces to surface tension. As *We* increase, the mixing in the coalesced drop is expected to intensify. However, the separation of drops after collision without coalescence easily occurs in the higher *We* condition [5]. Therefore, a novel manipulation method of drops should be developed to create an enhanced mixing field in the drop reactor.

One of the new methods for developing drop reactors is utilizing a unique drop motion on the superheated surface. When a water drop is dropped onto a superheated surface above its boiling temperature, the drop is levitated owing to the vapor generated by the instantaneous evaporation. Hence, the drop can exist for more than a few hundred seconds because the vapor cushion acts as a thermal insulator [6, 7]. This is called “Leidenfrost drop” and is observed for several types of liquid, e.g., alcohol [8], emulsion [9], refringent [10], and polymeric liquid [11]. Although the Leidenfrost drop has been investigated mainly in spray cooling [12], it is considered suitable for chemical reactors due to the high-intensity mixing field [13, 14] and the high-temperature field at approximately saturation temperature [15]. The Leidenfrost drop reactor has been applied to particle fabrication [16, 17] and organic synthesis [18]. However, the transient process of Leidenfrost drops during colliding, coalescence, and mixing, which are important topics for the initial stage of chemical reaction, is not fully understood. Compared with existing techniques of drop mixing [1-5], more intensified mixing is expected after the coalescence of Leidenfrost drops in even highly viscous drops due to the active internal flow.

Although several studies have investigated the internal flow and mixing characteristics of Leidenfrost droplets (e.g., Bouillant et al. [13] and Liu et al. [14]), these works did not address the collision and coalescence processes that are crucial for the initial stage of chemical reactions. In addition, in chemical reactions, reactants often have different thermophysical properties, such as density, viscosity, and saturated vapor pressure. In particular, mixing of high-viscosity or viscosity-contrasted fluids remains one of the long-standing challenges in chemical engineering [19]. When handling highly viscous fluids, the operation is often

constrained to laminar flow due to the large power requirement, making it difficult to achieve efficient mixing using conventional mechanically agitated systems such as stirred vessels. In contrast, the Leidenfrost drop reactor is expected to generate strong internal circulations driven by thermocapillary and vapor-flow-induced motion, enabling effective mixing even in highly viscous liquids.

Therefore, this study preliminarily investigates a series of phenomena—collision, coalescence, and mixing—between two Leidenfrost drops. Both small and large viscosity-ratio systems were examined to clarify the effect of viscosity contrast. Furthermore, the mixing performance was quantitatively evaluated from the viewpoint of energy efficiency and compared with that of a conventional stirred-tank reactor, thereby highlighting the unique potential of Leidenfrost drop reactors for process intensification.

2. MATERIALS AND METHODS

Figure 1 depicts the experimental setup. A stationary drop with an initial diameter (D_s) of 3.0 mm was first floated on a superheated duralumin plate (100 mm wide, 100 mm deep, and 20 mm thick) featuring a shallow spherical recess (200 mm radius and 2 mm depth). The plate was heated from below using a ceramic hot plate. The surface temperature was estimated based on the temperature measured at the mid-plane of the plate, 2 mm below the surface, using a 1 mm-diameter K-type sheathed thermocouple. Throughout the experiments, the surface temperature was maintained at 300°C. Although the surrounding environment, such as temperature and humidity, also affects the drop dynamics (e.g., evaporation) [20], these factors were not controlled in this study. The stationary drop preferably stayed in the center of the recess during experiments. Note that the slight curvature of the surface did not affect the drop dynamics [21]. After that, a colliding drop was dropped onto the superheated surface at some point distant from the center of the recess and rolled toward the stationary drop. In this study, two types of liquids were used as the stationary drop: Distilled water (DW) as the lowly viscous drop and 0.10 wt% xanthan gum aqueous solution (XG) as the highly viscous drop. In this study, assuming organic reactions, ethanol (Et), which has a smaller surface tension than DW and XG, was selected as the colliding drop. The diameter of the colliding drop, D_c, was 3.0 mm, which was the same diameter as the stationary drop. As physical properties of drops, viscosity (h), density (r), and surface tension (s) for each liquid were measured using a rheometer (MCR102, Anton Paar GmbH), a density meter (DA-640, Kyoto Electronics Manufacturing Co., Ltd.), and a contact angle meter (B100, ASUMI GIKEN Ltd.), respectively. Each measurement was carried out at 20°C as a reference value because of the difficulty of the measurements at the saturation temperature. These physical properties are highly temperature-dependent. Although it is desirable to evaluate them at the saturation temperature for more accurate analysis of drop dynamics, this is experimentally difficult. Therefore, the values at 20°C are used here as reference values. The rheological property of XG is shown in Figure 2, and it was confirmed that XG exhibits the typical shear-thinning behavior. The shear-thinning property was characterized by fitting the data to the Carreau model [22], which is described as follows:

$$\eta = (\eta_0 - \eta_\infty)[1 + (\beta \cdot \dot{\gamma})^2]^{\frac{n-1}{2}} + \eta_\infty \quad (1)$$

where, h_0 is the zero shear-rate viscosity, h_∞ is the infinite shear-rate viscosity, b is the characteristic time, $\dot{\gamma}$ is the shear-rate, and n is the power-law exponent. Note that this study primarily focused on the high viscosity of the polymeric drop, rather than the shear-thinning behavior exhibited by XG. While the shear-thinning property is an important factor in non-Newtonian fluids, the present research aimed to investigate the effects of high viscosity on drop dynamics. A comparison with a high-viscosity Newtonian fluid will be addressed in future work. The rheological parameters and other physical properties are summarized in Table 1.

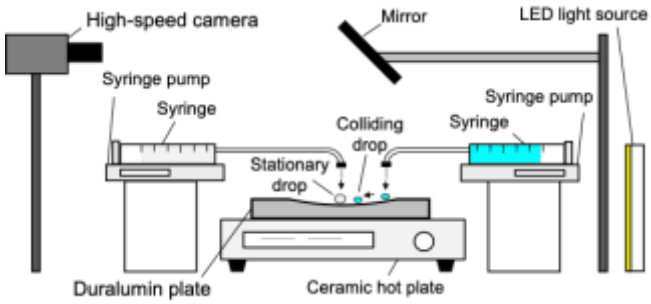

Figure 1. Experimental setup

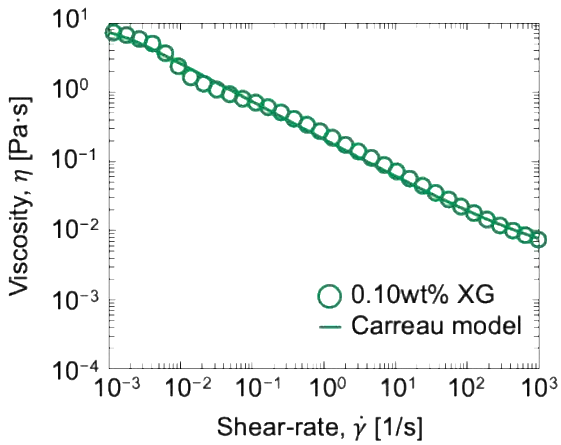

Figure 2. Rheological properties of 0.10 wt% XG

Table 1. Rheological parameters and physical properties of liquids

Liquid	Rheological Parameters				Physical Properties	
	Zero Shear-Rate Viscosity, h_0 [Pa·s]	Infinite Shear-Rate Viscosity, h_∞ [Pa·s]	Characteristic Time, b [s]	Power-Law Exponent, n [–]	Density, r [kg/m^3]	Surface Tension, s [mN/m]
DW	0.001	–	–	1	998.2	72.75
XG	8.7	0.004	900	0.45	998.3	70.95
Et	0.001	–	–	1	789.7	22.40

The colliding drop was colorized by adding a small amount of methylene blue. After collision and coalescence, the blue value decreased as mixing of the blue-colored colliding with the transparent stationary drops progressed. Hence, the mixing performance can be evaluated by measuring the change in the blue value over time. In stirred vessels, colorization (or decolorization) experiments using dye are commonly employed to determine the mixing time, defined as the time required to achieve a certain degree of homogeneity. Notably, this method does not focus on absolute color values, but rather on the time required to reach a sufficient level of homogeneity, as indicated by the color distribution. The validity of this colorimetric method for evaluating mixing time has been verified through comparison with other techniques, such as tracer-input experiments [23, 24]. Cabaret et al. [23] locally measured changes in red, green, and blue channel values during dye mixing and accurately determined the mixing time. Based on these precedents, this method was employed to determine the mixing time in Leidenfrost drops.

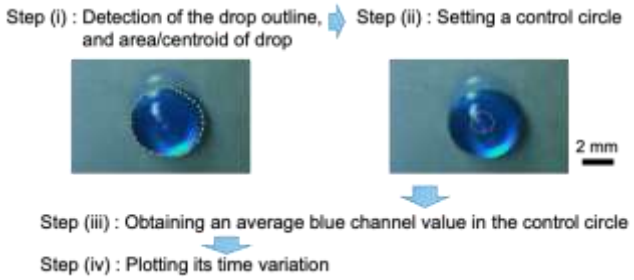

Figure 3. Overview of the image processing method used for mixing time evaluation in the coalesced drop

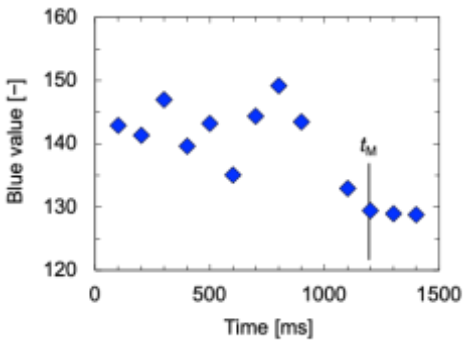

Figure 4. Time-course change of the blue channel value for the XG-Et system at We = 0.7

The drop dynamics during the experiments were observed and recorded from above via the mirror at 250 fps using a high-speed camera (HAS-U2, DITECT Corp.). The temporal change in the blue channel value within the drop was then analyzed through image processing using ImageJ software. As illustrated in Figure 3, the following procedure was employed to measure the mixing time: (i) The outline and centroid of the drop were detected from the top-view image, and its area was calculated; (ii) a control circle, occupying 10% of the total area, was placed concentrically at the drop center; (iii) the average blue channel value within this control circle was calculated; and (iv) its temporal variation was plotted. An example of the temporal change in the blue channel value within the coalesced drop is shown in Figure 4. As can be seen, the blue channel value asymptotically approached a stable value, despite some fluctuations in the early stage. After 1800 ms, these fluctuations became sufficiently small. In this study, the mixing time, t_M, was defined as the time after which the temporal fluctuation of the blue channel value remained within ±5% of the final value. The measurement was repeated several times, and the average value is reported in this paper.

By varying the distance of the initial injection point of the secondary drop, the We condition was controlled. We was defined based on the colliding drop (Et drop), as follows:

$$We = \frac{\rho_{Et} D_{Et} V_{Et}^2}{\sigma_{Et}} \tag{2}$$

where, r_{Et} is the ethanol density, D_{Et} is the diameter of the ethanol drop, V_{Et} is the colliding velocity of the ethanol drop to the stationary drop, and s_{Et} is the ethanol surface tension. V_{Et} was calculated from the recorded movie. The experiments were performed under We = 0.6 - 6.2. The drop collision phenomenon is also affected by an angle, which is formed between a line connecting the centers of two drops and the trajectory of the colliding drop [5]. In this study, the angle was 0 degrees, that is, the drops had a head-on collision in experiments.

The mixing performance of the Leidenfrost droplet system was compared with that of a traditional stirred vessel. Although the mixing efficiency of stirred vessels is known to depend strongly on operational conditions and geometrical configuration, the purpose of the present comparison is not to characterize the full performance range of stirred tanks but to provide a representative baseline for evaluating the relative mixing efficiency of the Leidenfrost system. Therefore, a widely used and standard configuration was selected. Figure 5 shows the experimental setup of the stirred vessel equipped with a Rushton turbine impeller, which is a common impeller type in laboratory and industrial mixing. Distilled water (DW) and xanthan gum (XG) solution were used as the working liquids, and the total liquid volume in the vessel was 1.30×10^{-3} m^3. In each experiment, a small amount of methylene blue aqueous solution was injected into the vessel while the impeller was rotated at 3.33 rps, which is a typical agitation speed for laboratory-scale vessels under the high-viscosity and thus low-Reynolds-number conditions of the XG solution. As mixing proceeded, the blue channel value in the vessel asymptotically approached a uniform level. The time required to reach this asymptotic value, as determined from the recorded video, was defined as the mixing time for the stirred vessel system. Additionally, the torque during mixing was measured using a torque meter (ST-3000II, SATAKE MultiMix Corp.).

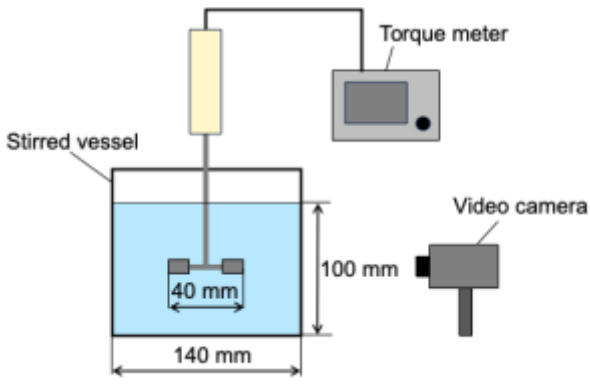

Figure 5. Experimental setup of a stirred vessel with a Rushton turbine impeller

3. RESULTS AND DISCUSSION

3.1 Collision and coalescence of Leidenfrost drops

Figure 6 shows a series of drop dynamics during collision, coalescence, and mixing at lower and higher *We* conditions. The results of the case for DW (colliding drop) and Et (stationary drop) drops at *We* = 1.3 and 6.2 are shown in Figure 6(a). In this case, the viscosity ratio of the two drops is close to 1. The time when the colliding drop was in contact with the stationary drop was designated as t = 0. At *We* = 1.3, the surface deformation of the colliding drop was small during the coalescing process (t = 8 – 24 ms), although the surface of the stationary drop slightly oscillated. This oscillation would be caused by the relatively lower viscous force and surface tension of the stationary drop, which was not enough to suppress the inertial force. After the coalescence, the distorted drop gradually returned to a sphere owing to the surface tension effect (t = 24 – 48 ms). At *We* = 6.2, the colliding drop was largely deformed due to the higher inertial force during the coalescing process (t = 4 – 20 ms), while the stationary drop kept the spheroid shape. The coalesced drop became the approximate spheroid (t = 20 – 24 ms) more rapidly than in the case of *We* = 1.3 and subsequently continued moving (t = 28 – 60 ms). This difference in the collision/coalescence pattern between lower and higher *We* conditions is analogous to that in the air[5] or on a superhydrophobic surface [25].

Figure 6(b) shows the results of the higher viscosity ratio cases for XG (colliding drop) and Et (stationary drop) at *We* = 1.1 and 5.7. At *We* = 1.1, the different dynamics from the lower viscosity ratio system were observed, that is, there was a delay after the colliding drop came into contact with the stationary drop until they coalesced (t = 0 - 20 ms). The delayed coalescence is also observed in the collision of two drops with a large viscosity or surface tension ratio in the air [4, 26]. Note that the delayed coalescence is not observed normally in the head-on collision of identical drops. Although there was no clear difference in the surface tension ratio, R_s, for each system (R_s ~ 3.25 for DW-Et and 3.17 for XG-Et), the delayed coalescence was not observed in the DW-Et system. Thus, it is inferred that the delayed coalescence in the XG-Et system at *We* = 1.1 originates in the viscosity ratio. Due to the shear-thinning property, the viscosity of XG drops depends on the shear rate, which is generated in collision/coalescence processes. Basically, to estimate an effective viscosity, the key issue is estimating the effective shear rate. For drop flows, the effective shear-rate, $\dot{\gamma}_{\mathrm{eff}}$, is estimated as V / D (V is the representative velocity and D is the drop diameter) [27]. Therefore, in this system, the effective shear-rate for the XG drop, $\dot{\gamma}_{\mathrm{eff}}$ was estimated as V_{Et} / D_{XG}. By substituting $\dot{\gamma}_{\mathrm{eff}} = V_{\mathrm{Et}}/D_{\mathrm{XG}}$ to the term of $\dot{\gamma}$ in Eq. (1), the effective viscosity, h_{eff}, is obtained, as shown in Eq. (3):

$$\eta_{\mathrm{eff}} = (\eta_0 - \eta_\infty)\left[1 + \left(\beta \cdot \frac{V_{\mathrm{Et}}}{D_{\mathrm{XG}}}\right)^2\right]^{\frac{n-1}{2}} + \eta_\infty \qquad (3)$$

As a result, the viscosity ratio, R_v (= h_s / h_c), for the XG-Et system was estimated to be approximately 22–39, depending on V_{Et}. Focke et al. [4] experimentally observed the delayed coalescence of drops with R_v ~ 23. Their system of drop collision is essentially different from this study; two drops having each velocity collided in the air at room temperature (i.e., no Leidenfrost effect) and higher *We* (~ 26); besides, the diameter of the drops was smaller (~ 0.7 mm). Nevertheless, the delayed coalescence was observed in a similar R_v condition, although *We* (~ 1) was much smaller than Focke's study [4]. According to Focke et al. [4], air is trapped between contacting drops with a large viscosity ratio and needs a certain time to leave the gap, although the detailed mechanism for air trapping is unclear. The mechanism proposed by Focke et al. [4] provides a useful analogy for interpreting the present observations; however, its direct applicability to Leidenfrost drop systems requires careful consideration. In the Leidenfrost state, a vapor layer continuously exists beneath the droplets, and additional vapor is generated upon collision. Therefore, the film between the colliding drops may consist of vapor rather than air, and its drainage dynamics could differ substantially from those in air collisions. Nevertheless, the observed delay in coalescence suggests that a similar film-rupture process might occur, governed by the interplay between vapor flow, viscosity ratio, and impact inertia. In Focke et al.'s study [4], they assumed that the delayed coalescence is attributed to the rupture of the thin air film between drops. Therefore, the delayed time is considered shorter at higher collision velocity because a higher inertial force destabilizes the thin air film, as analytically indicated by Krishnan and Loth [28]. They assumed that the delayed coalescence is attributed to the rupture of the thin air film between drops. Therefore, the delayed time is considered shorter at higher collision velocity because a higher inertial force destabilizes the thin air film, as analytically indicated by Krishnan and Loth [28]. In our experiments, at higher *We* (e.g., *We* = 5.7), the obvious delay was not observed, and drops immediately coalesced, as shown in Figure 6(b). In addition, there was no large deformation of the colliding Et drop, differing from the DW-Et system. This result suggests that the viscosity ratio between the colliding and stationary drops suppresses the drop deformation, leading to smooth coalescence. In addition, as reported by Qian et al. [29], the non-Newtonian properties of the fluid can influence the evolution of kinetic and surface energies during drop coalescence. Therefore, for a more complete understanding, not only the viscosity ratio but also the non-Newtonian behavior should be considered in future investigations.

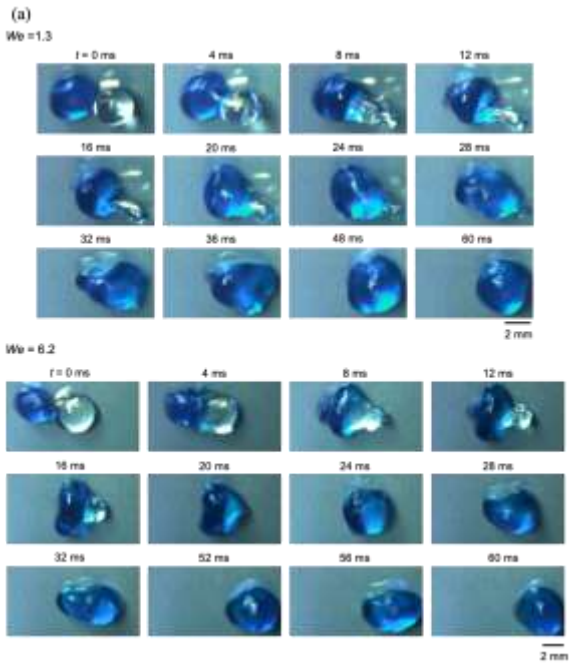

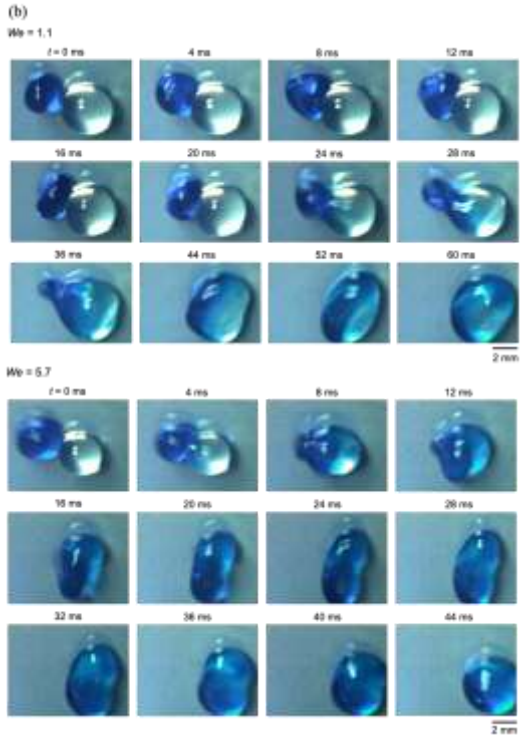

Figure 6. Drop dynamics after contact: (a) DW–Et system, and (b) XG–Et system

Figure 7 shows the delayed time until coalescence, t_d, in the XG-Et system with *We*. Note that the delay shorter than 4 ms could not be detected due to the limitation of the camera capability (250 fps); hence, if the delayed coalescence is not observed above for 4 ms, no delay (i.e., $t_d = 0$) was assumed. The delayed time tended to decrease with *We*, as shown in Figure 7. This decrease in the delayed coalescence time with increasing *We* can be interpreted in terms of the dynamics of the thin film between the drops. A larger *We* corresponds to a higher impact velocity, which increases the dynamic pressure acting on the film (approximately $\sim\rho V^2$). This enhanced pressure accelerates the drainage of the vapor layer trapped between the two drops. The characteristic drainage time is expected to decrease with increasing dynamic pressure and is therefore shortened at higher *We*. In addition, the higher inertial force at large *We* amplifies interfacial deformation, leading to a locally reduced film thickness and promoting interfacial instabilities that facilitate film rupture. As a result, the thin film becomes unstable more rapidly and the coalescence initiates earlier. This dynamical interpretation is consistent with the trends observed in previous studies by Focke et al. [4].

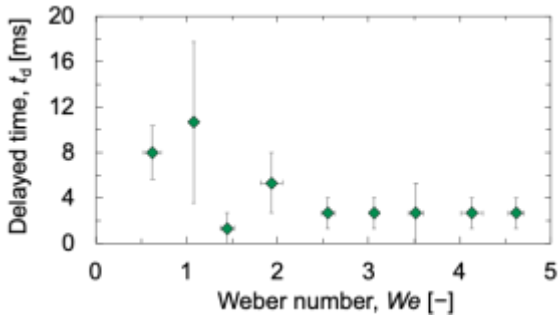

Figure 7. Effect of Weber number on the delayed time for drop coalescence in the XG-Et system

Moreover, it was confirmed that the delayed coalescence occurs at relatively lower conditions, $We \leq 2$. This indicates that the thin air film is easily ruptured (i.e., more unstable) compared to the study by Focke et al. [4] in which the delayed coalescence was observed even at the higher *We* (~26). Evidently, the stability of thin air film is affected by the vapor generated from the side surface of the Leidenfrost drops (i.e., the contact surface of the drops) [30]. Although this effect was not directly measured in the present study, it is reasonable to consider that vapor flow and pressure dynamics influence the coalescence behavior. A more quantitative investigation, including direct measurement of vapor-film evolution, will be required to clarify this mechanism in future work. Further experiments varying parameters such as viscosity ratio, diameter ratio, and surface temperature will be necessary to understand the detailed mechanism of drop coalescence. In addition, numerical simulations would be a powerful approach to elucidate the detailed mechanisms of delayed coalescence, as they enable the analysis of local velocity and pressure fields at the liquid–gas–liquid interfaces during the coalescence process.

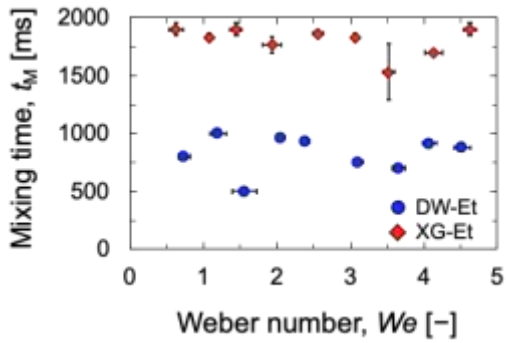

Figure 8. Effect of mixing time on Weber number in the Leidenfrost drops system

Figure 8 indicates the effect of *We* on mixing time (t_M) for each system (DW-Et and XG-Et). The mixing time can be considered constant in each system, although there is a certain variation with *We*; the average t_M is 822 ms for the DW-Et system and 1810 ms for the XG-Et system. This tendency of no clear dependence of t_M on *We* suggests that, under the range of *We* examined in this study, the convection generated within the drop after coalescence was sufficient to promote mixing, even at lower *We*. It is also possible that internal flow driven by evaporation contributed to the observed mixing behavior. The weak dependence of the mixing time t_M on *We* can be interpreted by comparing the characteristic time scales of the internal flow. The large-scale motion induced directly by the collision can be characterized by an advective time scale $t_{ad} \sim D/V$. For the present conditions, t_{ad} is on the order of 10^1 ms. The subsequent relaxation of the deformed droplet shape is governed by a capillary time scale $t_{ca} \sim \sqrt{\rho D^3/\sigma}$, which is typically on the order of 10^2 ms. Both of these are much shorter than the measured mixing time, which is on the order of 10^3 ms. This separation of time scales implies that the impact-induced flow and the capillary relaxation process are relatively short-lived compared with the overall mixing process, and thus their direct contribution to the total mixing time is limited. Instead, the mixing is likely dominated by more sustained convection driven by vapor-flow-induced circulation inside the Leidenfrost drop, whose characteristic intensity is expected to depend only weakly on *We* within the present

range. To verify these assumptions, future studies should include direct observation of internal flow using appropriate techniques, such as particle image velocimetry (PIV) or numerical simulations. While stronger internal convection might occur at higher *We*, our preliminary observations revealed that such conditions often result in drop separation rather than stable coalescence. For practical applications as a mixing device, it is therefore desirable to perform collisions at relatively low *We* (e.g., *We* ≤ 5). In addition to the effect of collision conditions, physicochemical changes within the droplet may also influence the mixing behavior. As the ethanol drop undergoes evaporation, preferential loss of more volatile components could lead to a compositional change, potentially affecting the surface tension and internal flow. Although the mixing time was relatively short in the experiments, this effect was not directly evaluated in the present study. Nevertheless, it may influence the observed mixing dynamics and should be addressed in future investigations.

The difference in t_M between systems would result from the difference in the viscosity because a higher viscous force suppresses convection. In addition, the delayed coalescence in the XG-Et system is negligible for the mixing performance because its time scale is sufficiently shorter than that of the mixing.

3.2 Mixing efficiency of Leidenfrost drops

Based on the power consumption per liquid volume, the mixing efficiency of the Leidenfrost drops was evaluated by comparison with the stirred vessel. Accurately estimating the energy consumption for mixing in Leidenfrost drop systems is not apparent because much energy was radiated in the air; in other words, how much energy was input from the heater to the drops is unclear. Hence, the energy consumption was estimated by the mass loss of the coalesced drop during the mixing experiment, assuming that the input energy was completely converted to the latent energy (i.e., vapor generation). By assuming that heat brought to the drop is transferred by heat conduction through the vapor film [6], the mass change of Leidenfrost drops with time is expressed by:

$$\frac{dm}{dt} = \frac{1}{L}\kappa\frac{\Delta T}{h}\pi\lambda^2 \tag{4}$$

where, m is the mass of the drop, L is the latent heat of evaporation, k is the thermal conductivity of the vapor, DT is the temperature difference between the surface temperature (T_s) and the boiling temperature (T_b) of the liquid, h is the vapor film thickness, and pl^2 is the effective heat transfer area of the drop. In Eq. (4), radiative and convective heat transfer were neglected. The radiative heat flux, q_r, is expressed by:

$$q_r = e\sigma_{SB}(T_s^4 - T_b^4) \tag{5}$$

where, e is the emissivity, and s_{SB} is the Stefan-Boltzmann constant. Considering the variation in emissivity due to the surface condition of duralumin [31], q_r is estimated to be approximately 400–3300 W/m^2. In contrast, the conductive heat flux ($q_c = k$ DT / h) is estimated to be approximately 6.4 × 10^4 - 6.4 × 10^5 W/m^2, assuming h on the order of 10^{-5} to 10^{-6} m [32]. These estimates indicate that q_c is significantly larger than q_r. Furthermore, convective heat transfer through the vapor layer between the drop and the heated surface is considered negligible due to the low Reynolds number of the vapor flow. In fact, the vapor flow can be analyzed using lubrication theory under such low-Reynolds-number conditions [6]. Therefore, the assumption for neglecting radiative and convective heat transfer can be considered reasonable.

Based on a balance between gravity and surface tension [33], l is given as:

$$\lambda \sim \left(\frac{D}{2}\right)^2 \frac{1}{a} \sim \left(\frac{D}{2}\right)^2 \sqrt{\frac{\rho g}{\sigma}} \tag{6}$$

where, a is the capillary length. Biance et al. [6] derived the vapor film thickness, as follows:

$$h = \left(\frac{3\kappa\Delta T\eta_v}{4L\rho_v\rho g a}\right)^{\frac{1}{4}}\left(\frac{D}{2}\right)^{\frac{1}{2}} \tag{7}$$

where, h_v is the vapor viscosity and r_v is the vapor density. Besides, they derived the drop diameter change with time [6], as follows:

$$D(t) = D_0\left(1 - \frac{t}{\tau}\right)^2 \tag{8}$$

With

$$\tau = 2\left(\frac{4\rho a L}{\kappa\Delta T}\right)^{\frac{3}{4}}\left(\frac{3\eta}{\rho_v g}\right)^{\frac{1}{4}}\left(\frac{D_0}{2}\right)^{\frac{1}{2}} \tag{9}$$

According to Biance et al. [6], Eqs. (8) and (9) accurately predict the size decrease in one drop under the Leidenfrost state. However, in their experiments, there was no collision and coalescence, that is, a relatively static condition. Hence, its validity for the "dynamic" Leidenfrost drop was examined by comparing the change in the drop size in our experimental data with predicted values from Eqs. (8) and (9). Because the coalesced drop during mixing was far from a sphere, as indicated in Figure 6, its diameter is not measured directly. Thus, based on the similar procedure shown in Figure 3, an equivalent drop diameter from the area of the recorded image from above was calculated as the representative size. The change in the drop diameter for experiments and prediction is shown in Figure 9. Note that the diameter shown in Figure 9 was normalized by the equivalent diameter at the initial coalescence stage. Figure 9 indicates that the experimental results show good agreement with predicted values estimated from the model for "static" Leidenfrost drops (Eqs. (8) and (9)), although there was a slight deviation. Thus, the model is considered applicable for dynamic Leidenfrost drops.

By combining Eqs. (4), (6)-(9), the mass loss during mixing, Dm_M, can be estimated as follows:

$$\Delta m_M = \int_0^{t_M} \frac{1}{L}\kappa \frac{\Delta T}{\left(\frac{3\kappa\Delta T\eta_v}{4L\rho_v\rho g a}\right)^{\frac{1}{4}}\left(\frac{D(t)}{2}\right)^{\frac{1}{2}}}\pi\left(\frac{D(t)}{2}\right)^4\left(\frac{\rho g}{\sigma}\right)dt \tag{10}$$

As a result, the energy consumption per unit mass, ε, for the drop system is obtained by:

$$\varepsilon = \frac{\Delta m_M L}{t_M \rho\left(\frac{\pi D_0^3}{6}\right)} \tag{11}$$

Because there are no data on some thermophysical properties of XG at the saturated temperature, those of DW

were used for estimation of ε. Furthermore, based on energy consumption, the mixing efficiency of Leidenfrost drops was compared with stirred vessel systems. The energy consumption per unit mass for the stirred vessel was obtained by

$$\varepsilon = \frac{\int_0^{t_M} 2\pi n_s T dt}{\rho V_l} \tag{12}$$

where, n_s [rps] is the agitation speed (n_s = 3.33 rps) and V_l [m^3] is the liquid volume ($V_l = 1.30 \times 10^{-3}$ m^3).

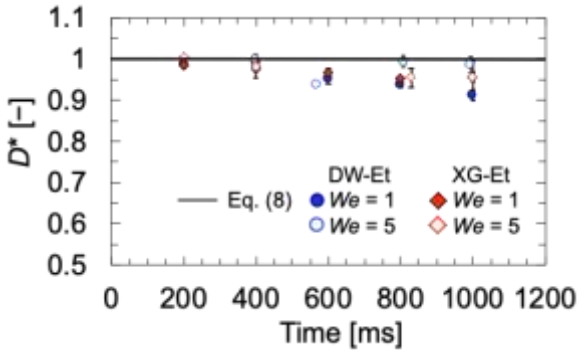

Figure 9. Comparison between experimental and model non-dimensional equivalent drop diameters

The mixing performance of each system is summarized in Table 2. A significantly shorter mixing time was obtained using Leidenfrost drops compared with the traditional methods, i.e., the stirred vessel. In particular, rapid mixing was realized even in the XG-Et system, which has a large viscosity ratio. Thus, the viscosity difference between liquids caused no trouble in the Leidenfrost drops mixer. Besides, there was no clear difference between each system in the power input (ε). In the high viscosity liquid mixing using the stirred vessel, more larger power input is required because of larger energy dissipation near the fixed walls. Besides, a poor mixing region is often formed. Therefore, Leidenfrost drops are an effective technique for high viscosity liquid mixing due to no further power input requirement. One of the reasons for this is that the drop is contactless with any walls, that is, it is free from friction. However, the Leidenfrost mixer has inherent limitations, including low throughput and relatively high energy consumption due to the need for continuous surface heating. Nevertheless, it may be well-suited for applications that demand rapid mixing and the synthesis of high-value-added materials, particularly in scenarios where small-scale or localized processing is acceptable. However, the Leidenfrost drop reactor has inherent limitations, including low throughput and relatively high energy consumption due to the need for continuous surface heating. Even so, it may still offer advantages in specific contexts where rapid mixing of small liquid volumes is required. Examples include laboratory-scale material synthesis, rapid screening processes, or droplet-based operations in microreactor or lab-on-a-chip environments. In such cases, localized and fast mixing is often prioritized over throughput. A detailed evaluation of economic feasibility or application-specific requirements is beyond the scope of the present study and should be examined in future work.

To improve the throughput, utilizing a self-propelled Leidenfrost drop would be a solution. On the ratchet-shaped superheated surface, the drop moves in one direction [34]. By continuously dropping multiple drops onto the ratchet-shaped surface, continuous operations such as mixing and reaction can be carried out; consequently, the throughput is increased. Reduction in energy consumption is also crucial because a certain amount of energy is indispensable for the generation of vapor. Recently, it has been reported that the drop levitates at a lower temperature on the microstructured surface [35]. By applying this finding, the reduction in ε is expected due to realizing the Leidenfrost state at the lower temperature. Thus, although there are some subjects, the Leidenfrost drop is a new technology for fast mixing regardless of the liquid viscosity.

Table 2. Mixing the performance of each system

	ε [W/kg]	t_M [s]	Volume [m^3]
Leidenfrost drops			
DW–Et system (low viscosity liquid mixing)	4.2×10^4	0.82	1.41×10^{-8}
XG–Et system (high viscosity liquid mixing)	4.2×10^4	1.81	1.41×10^{-8}
Stirred vessel			
DW system (low viscosity liquid mixing)	7.4×10^1	45	1.30×10^{-3}
XG system (high viscosity liquid mixing)	2.0×10^2	110	1.30×10^{-3}

4. CONCLUSIONS

The collision, coalescence, and mixing processes of two Leidenfrost drops with or without a viscosity ratio were investigated based on visualization experiments. In experiments, the ethanol (Et) drop collided with the stationary drop of distilled water (DW) or 0.1 wt% xanthan gum aqueous solution (XG) on the superheated surface. By colorizing the Et drop with methylene blue, the mixing performance was evaluated by the change in blue value.

Within the experimental ranges of Weber number, the Et drop immediately coalesced with the water drop after the collision. On the contrary, in the XG-Et drop system, drops were not instantaneously coalesced; that is, the delayed coalescence was observed. Although the viscosity ratio of the stationary and collision drops would result in the delayed coalescence, the detailed mechanism is still unclear. The time scale of the delay in coalescence was much smaller than the mixing time, which was estimated from the recorded movies. Therefore, the delayed coalescence has little effect on the mixing performance. It was found that the mixing time strongly depends not on the Weber number but on the species of the stationary drop. In the XG-Et system, the mixing time was approximately 2.2 times longer than in the DW-Et system. This difference in the mixing time was caused by suppressing the active internal convection within the drop by a higher viscous force. Nevertheless, the rapid mixing (~1 s) was performed even in the XG-Et system.

The mixing efficiency of Leidenfrost drops was compared with stirred vessel systems based on the energy consumption per liquid volume. Regarding the efficiency of stirred vessels, the data in the literature were used. Although mixing in Leidenfrost drops was carried out in a very short time, there were disadvantages compared with stirred vessel systems: (i)

the net throughput is significantly small, and (ii) much energy is required. These disadvantages should be overcome by the increase in throughput and the reduction in the Leidenfrost temperature in the future. However, the increase in required energy with the viscosity was negligible, unlike stirred vessel systems, because the drop is free from friction by levitating on the vapor cushion. Therefore, it can be concluded that the Leidenfrost drop mixer can potentially enhance the mixing of high viscosity liquids. In the future, the mixing process of two Leidenfrost drops, including the internal flow, should be investigated under wider conditions (surface temperature, polymer concentration, and drop diameters). Moreover, when polymeric drops are used to represent high-viscosity fluids, the effects of non-Newtonian properties—such as shear-thinning behavior and viscoelasticity—on drop dynamics become important. Therefore, as part of future work, experiments using other types of polymers and non-Newtonian fluids will be conducted to investigate these effects in more detail.

ACKNOWLEDGMENT

This research was partially supported by JSPS KAKENHI (Grant numbers: 21KK0261, 23K13592, and 25K08368). The authors would like to thank Prof. Dieter Bothe (Technical University of Darmstadt) for the helpful discussion about drop collision/coalescence.

REFERENCES

[1] Nightingale, A.M., Phillips, T.W., Bannock, J.H., de Mello, J.C. (2014). Controlled multistep synthesis in a three-phase droplet reactor. Nature Communications, 5(1): 3777. https://doi.org/10.1038/ncomms4777

[2] Thoni, L., Klemmed, B., Georgi, M., Benad, A., Klosza, S., Eychmüller, A. (2020). Continuous droplet reactor for the production of millimeter sized spherical aerogels. RSC Advances, 10(4): 2277-2282. https://doi.org/10.1039/C9RA09631K

[3] Niu, G., Zhang, L., Ruditskiy, A., Wanh, L., Xia, Y. (2018). A droplet-reactor system capable of automation for the continuous and scalable production of noble-metal nanocrystals. Nano Letters, 18(6): 3879-3884. https://doi.org/10.1021/acs.nanolett.8b01200

[4] Focke, C., Kuschel, M., Sommerfeld, M., Bothe, D. (2013). Collision between high and low viscosity droplets: Direct numerical simulations and experiments. International Journal of Multiphase Flow, 56: 81-92. https://doi.org/10.1016/j.ijmultiphaseflow.2013.05.008

[5] Gao, T.C., Chen, R.H., Pu, J.Y., Lin, T.H. (2005). Collision between an ethanol drop and a water drop. Experiments in Fluids, 38(6): 731-738. https://doi.org/10.1007/s00348-005-0952-1

[6] Biance, A.L., Clanet, C., Quéré, D. (2023). Leidenfrost drops. Physics of Fluids, 15(6): 1632-1637. https://doi.org/10.1063/1.1572161

[7] Quéré, D. (2013). Leidenfrost dynamics. Annual Review of Fluid Mechanics, 45(1): 197-215. https://doi.org/10.1146/annurev-fluid-011212-140709

[8] Cai, C., Liu, H., Chen, H., Si, C. (2023). Alcohol-induced elevation in the dynamic Leidenfrost point temperature for water droplet impact. International Journal of Heat and Mass Transfer, 215: 124483. https://doi.org/10.1016/j.ijheatmasstransfer.2023.124483

[9] Lyu, S., Tan, H., Wakata, Y., Yang, X., Law, C.K., Lohse, D., Sun, C. (2021). On explosive boiling of a multicomponent Leidenfrost drop. Proceedings of the National Academy of Sciences, 118(2): e2016107118. https://doi.org/10.1073/pnas.2016107118

[10] Linke, H., Alemán, B.J., Melling, L.D., Taromina, M.J., Francis, M.J., Dow-Hygelund, C.C., Narayanan, V., Taylor, R.P., Stout, A. (2006). Self-propelled Leidenfrost droplets. Physical Review Letters, 96(15): 154502. https://doi.org/10.1103/PhysRevLett.96.154502

[11] Masuda, H., Wada, K., Okumura, S., Iyota, H. (2023). Dynamics of a polymer solution droplet on a high-temperature surface. Chemical Engineering and Technology, 46(9): 1756-1762. https://doi.org/10.1002/ceat.202300065

[12] Liang, G., Mudawar, I. (2017). Review of spray cooling – Part 1: Single-phase and nucleate boiling regimes, and critical heat flux. International Journal of Heat and Mass Transfer, 115: 1174-1205. https://doi.org/10.1016/j.ijheatmasstransfer.2017.06.029

[13] Bouillant, A., Mouterde, T., Bourrianne, P., Lagarde, A., Clamet, C., Quéré, D. (2018). Leidenfrost wheels. Nature Physics, 14(12): 1188-1192. https://doi.org/10.1038/s41567-018-0275-9

[14] Liu, M., Ji, B., Dang, C., Zhao, F., Zhang, C., Jin, Y., Jiang, M., Lu, Y., Tang, H., Wang, S., Wang, Z. (2024). Leidenfrost effect-induced chaotic vortex flow for efficient mixing of highly viscous droplets. Advanced Materials, 36(40): 2409192. https://doi.org/10.1002/adma.202409192

[15] Rueda Villegas, L., Tanguy, S., Castanet, G., Caballina, O., Lemoine, F. (2017). Direct numerical simulation of the impact of a droplet onto a hot surface above the Leidenfrost temperature. International Journal of Heat and Mass Transfer, 104: 1090-1109. https://doi.org/10.1016/j.ijheatmasstransfer.2016.08.105

[16] Abdelaziz, R., Disci-Zayed, D., Hedayati, M.K., Pöhls, J.H., Zillohu, A.U., Erkartal, B., Chakravadhanula, V.S. K., Duppel, V., Kienle, L., Elbahri, M. (2013). Green chemistry and nanofabrication in a levitated Leidenfrost drop. Nature Communications, 4(1): 2400. https://doi.org/10.1038/ncomms3400

[17] Liu, Z., Liu, Y., Yang, J., Li, S., Peng, C., Cui, X., Sheng, L., Wu, B. (2022). Highly efficient and controlled fabrication of supraparticles by Leidenfrost phenomenon. Langmuir, 38(30): 9157-9165. https://doi.org/10.1021/acs.langmuir.2c00709

[18] Bain, R.M., Pulliam, C.J., Thery, F., Cooks, R.G. (2016). Accelerated chemical reactions and organic synthesis in Leidenfrost droplets. Angewandte Chemie International Edition, 55(35): 10478-10482. https://doi.org/10.1002/anie.201605899

[19] Kresta, S.M., Krebs, R., Martin, T. (2004). The future of mixing research. Chemical Engineering and Technology, 27(3): 208-214. https://doi.org/10.1002/ceat.200402020

[20] Fujita, A., Kurose, R., Komori, S. (2010). Experimental study on effect of relative humidity on heat transfer of an evaporating water droplet in air flow. International Journal of Heat and Mass Transfer, 36: 244-247. https://doi.org/10.1016/j.ijmultiphaseflow.2009.10.004

[21] Hidalgo-Caballero, S., Escobar-Ortega, Y., Pacheco-Vázquez, F. (2016). Leidenfrost phenomenon on conical

surfaces. Physical Review Fluids, 1(5): 051902. https://doi.org/10.1103/PhysRevFluids.1.051902
[22] Carreau, P.J. (1972). Rheological equations from molecular network theories. Transactions of the Society of Rheology, 16(1): 99-127. https://doi.org/10.1122/1.549276
[23] Cabaret, F., Bonnot, S., Fradette, L., Tanguy, P.A. (2007). Mixing time analysis using colorimetric methods and image processing. Industrial and Engineering Chemistry Research, 46(14): 5032-5042. https://doi.org/10.1021/ie0613265
[24] Rosseburg, A., Fitschen, J., Wutz, J., Wucherpfennig, T., Schlüter, M. (2018). Hydrodynamic inhomogeneities in large scale stirred tanks – Influence on mixing time. Chemical Engineering Science, 188: 208-220. https://doi.org/10.1016/j.ces.2018.05.008
[25] Li, S., Chu, F., Zhang, J., Brutin, D., Wen, D. (2020). Droplet jumping induced by coalescence of a moving droplet and a static one: Effect of initial velocity. Chemical Engineering Science, 211: 115252. https://doi.org/10.1016/j.ces.2019.115252
[26] Chen, R.H., Chen, C.T. (2006). Collision between immiscible drops with large surface tension difference: Diesel oil and water. Experiments in Fluids, 41(3): 453-461. https://doi.org/10.1007/s00348-006-0173-2
[27] Ohta, M., Iwasaki, E., Obata, E., Yoshida, Y. (2005). Dynamic processes in a deformed drop rising through shear-thinning fluids. Journal of Non-Newtonian Fluid Mechanics, 132(1-3): 100-107. https://doi.org/10.1016/j.jnnfm.2005.10.008
[28] Krishnan, K.G., Loth, E. (2015). Effects of gas and droplet characteristics on drop-drop collision outcome regimes. International Journal of Multiphase Flow, 77: 171-186. https://doi.org/10.1016/j.ijmultiphaseflow.2015.08.003
[29] Qian, L., Liu, X., Zhu, C. (2024). Binary collision dynamics of immiscible Newtonian and non-Newtonian fluid droplets. Physics of Fluids, 36(11): 113107. https://doi.org/10.1063/5.0239205
[30] Pacheco-Vázquez, F., Ledesma-Alonso, R., Palacio-Rangel, J.L., Moreau, F. (2021). Triple Leidenfrost effect: Preventing coalescence of drops on a hot plate. Physical Review Letters, 127(20): 204501. https://doi.org/10.1103/PhysRevLett.127.204501
[31] Holman, J. (2010). Heat Transfer. The McGraw-Hill Companies, USA, New York, pp. 663-664.
[32] Lee, G.C., Noh, H., Kwak, H.J., Kim, T.K., Park, H.S., Fezzaa, K., Kim, M.H. (2018). Measurement of the vapor layer under a dynamic Leidenfrost drop. International Journal of Heat and Mass Transfer, 124: 1163-1171. https://doi.org/10.1016/j.ijheatmasstransfer.2018.04.050
[33] Mahadevan, L., Pomeau, Y. (1999). Rolling droplets. Physics of Fluids, 11(9): 2449-2453. https://doi.org/10.1063/1.870107
[34] Masuda, H., Okumura, S., Wada, K., Iyota, H. (2024). Self-propelled polymeric droplet in Leidenfrost state on a superheated ratchet surface. Industrial and Engineering Chemistry Research, 63(15): 6785-6793. https://doi.org/10.1021/acs.iecr.4c00056
[35] Tran, T., Staat, H.J.J., Susarrey-Arec, A., Foertsch, T.C., van Houselt, A., Gardeniers, H.J.G.E., Prosperetti, A., Lohse, D., Sun, C. (2013). Droplet impact on superheated micro-structured surfaces. Soft Matter, 9(12): 3272-3282. https://doi.org/10.1039/C3SM27643K